

Agentic AI for Scalable and Robust Optical Systems Control

Zehao Wang*, Mingzhe Han*, Wei Cheng, Yue-Kai Huang, Philip Ji, Denton Wu, Mahdi Safari, Flemming Holtorf, Kenaish AlQubaisi, Norbert M. Linke, Danyang Zhuo, Yiran Chen, Ting Wang, Dirk Englund, and Tingjun Chen

Abstract—We present AgentOptics, an agentic AI framework for high-fidelity, autonomous optical system control built upon the model context protocol (MCP). AgentOptics interprets natural language tasks and executes protocol-compliant actions on heterogeneous optical devices through a structure tool abstraction layer. We implement 64 standardized MCP tools spanning eight representative optical devices and construct a comprehensive 410-task benchmark to evaluate the performance of AgentOptics across request understanding, role-dependent responses, multi-step coordination, robustness to linguistic variation, and error-handling capability. We evaluate two deployment configurations—integrating either commercial online large language models (LLMs) or locally hosted open-source LLMs—and compare against LLM-based code generation baselines. Experimental results demonstrate that AgentOptics achieves 87.7%–99.0% average task success rates, significantly outperforming code generation approaches with up to only 50% success rate. We further validate the broader applicability of AgentOptics through five representative case studies that extend beyond accurate device control to enable system-level orchestration and monitoring, as well as closed-loop optimization. These case studies include dense wavelength division multiplexing (DWDM) link provisioning and coordinated performance monitoring of coherent 400 GbE and analog radio-over-fiber (ARoF) channels, autonomous characterization and bias optimization of a wideband ARoF link carrying 5G fronthaul traffic, multi-span channel provisioning and signal launch power optimization, closed-loop fiber link polarization stabilization, and distributed acoustic sensing (DAS)-based fiber

monitoring with LLM-assisted event interpretation and detection. These results demonstrate that AgentOptics provides a scalable and robust paradigm for autonomous control and orchestration of heterogeneous optical devices and systems.

Index Terms—Agentic AI, optical networks, networked system control, closed-loop automation, large language models

I. INTRODUCTION

Optical networks form the backbone of modern Internet infrastructure, interconnecting data centers, metro and long-haul transport systems, wireless front/backhaul, and emerging quantum networks [1]–[8]. As optical systems scale in both heterogeneity and performance—incorporating reconfigurable optical add-drop multiplexer (ROADMs), coherent pluggable transceivers, radio-over-fiber (RoF) links, as well as fiber sensing and quantum photonic hardware—the operational complexity of device configuration, monitoring, and optimization increase significantly. Achieving high fidelity, reliability, and efficiency in these systems requires coordinated control across heterogeneous devices, accommodation of vendor-specific management interfaces, and closed-loop telemetry and adaptation mechanisms.

Software-defined networking (SDN) has been widely adopted in optical networks to decouple the control plane from the data transmission plane, enabling centralized control, programmability, and automated provisioning of optical resources [5], [9]–[11]. By abstracting network control, SDN improves operational efficiency and flexibility in managing complex optical infrastructures. Initiatives such as OpenROADM [12] also aim to address this challenge by defining common data models and standardized control interfaces across multi-vendor optical transport equipment, improving system interoperability and manageability.

However, existing SDN solutions face limitations in multi-vendor environments due to inconsistent support for standardized interfaces and vendor-specific extensions. In addition, limited abstraction of physical-layer behaviors and device capabilities increases system complexity and poses challenges for operators seeking scalable and intuitive network control. In current practice, SDN low-level control layers often rely on human-written scripts derived from vendor manuals or implemented through software development kits (SDK) and command-line interface (CLI) tools, as illustrated in Fig. 1(a). Developers and users must translate high-level experimental goals (e.g., “get optical power spectrum”) into explicit sequences of function calls or protocol commands (e.g., via

This work has been submitted to the IEEE for possible publication. Copyright may be transferred without notice, after which this version may no longer be accessible.

This work was supported in part by NSF under grants EEC-1941583, CNS-2112562, OIA-2134891, CNS-2211944, PHY-2325080, CNS-2330333, CNS-2443137, CNS-2450567, and OAC-2503010, and ARO under grant W911NF2510241. We also acknowledge funding from Duke University under the Beyond-the-Horizon and DST-Launch initiatives. *These authors contributed equally to this work.

Z. Wang, M. Han, W. Cheng, Y. Chen, and T. Chen are with the Department of Electrical and Computer Engineering, Duke University, Durham, NC 27708, USA (email: {zehao.w, mingzhe.han, wei.cheng, yiran.chen, tingjun.chen}@duke.edu).

D. Wu is with the Duke Quantum Center and Department of Physics, Duke University, Durham, NC, USA 27708 (email: denton.wu@duke.edu).

D. Zhuo is with the Department of Computer Science, Duke University, Durham, NC 27708, USA (email: danyang@duke.edu).

Y.-K. Huang, P. Ji, and T. Wang are with NEC Laboratories America, Princeton, NJ 08540, USA (email: {kai, pji, ting}@nec-labs.com).

M. Safari and F. Holtorf are with Axiomatic AI, Cambridge, MA 02139, USA (email: {mahdi, flemming}@axiomatic-ai.com).

N. Linke is with the Joint Quantum Institute, Department of Physics, and the National Quantum Laboratory (QLab), University of Maryland, College Park, MD 20742, USA; the Duke Quantum Center and Department of Physics, Duke University, Durham, NC 27708, USA; (email: linke@umd.edu).

D. Englund and K. AlQubaisi are with the Research Laboratory of Electronics, Massachusetts Institute of Technology, Cambridge, MA 02139, USA (email: {englund, alalif}@mit.edu).

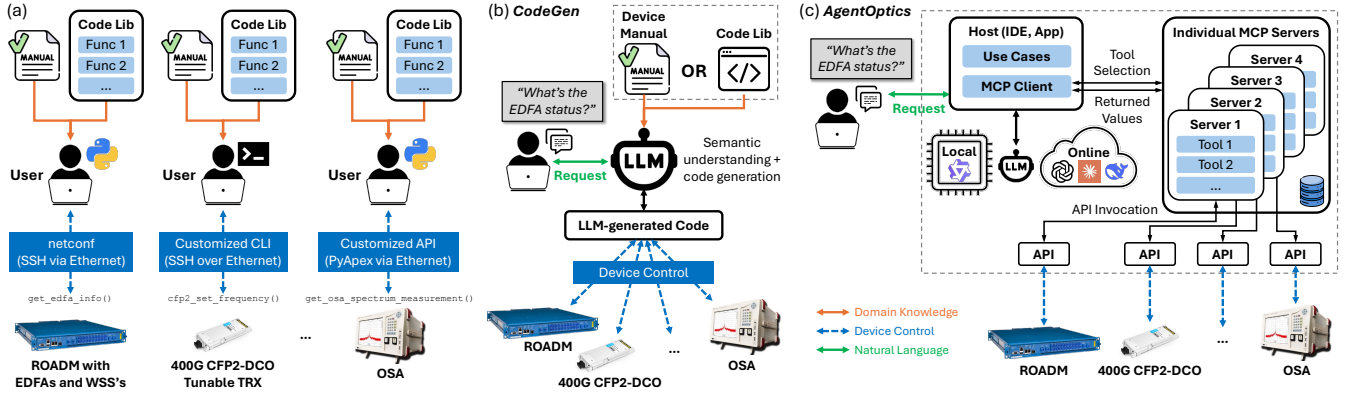


Fig. 1: Traditional optical device control using ROADM, 400 GbE CFP2-DCO, and OSA as examples: (a) Traditional control requires device-specific manuals, custom scripts, and protocol handling. (b) LLM-based control interprets natural-language prompts to generate control code, reducing manual scripting. (c) The proposed AgentOptics framework standardizes control via a unified tool layer, where the MCP client maps prompts to device APIs through tool selection, enabling LLM-based reasoning over tool outputs for more autonomous control.

NETCONF/SSH or vendor-provided Python APIs), manually specify execution order, establish device connections, validate parameter constraints, and parse raw device responses. While this workflow offers precise control, it requires substantial engineering work and device-specific expertise, resulting in significant onboarding effort and limited portability across heterogeneous equipment.

Recent advances in large language models (LLMs) have enabled intuitive, natural language-based interaction with complex systems, transforming how users control, configure, and automate technical workflows [13]. The primary advantage of LLM-based agents is not merely improved natural language understanding, but the ability to translate high-level design objectives into structured, multi-step execution workflows, augmented with reasoning and decision-making capabilities. However, enabling reliable interaction between LLMs and heterogeneous technical systems requires more than improved reasoning capability: it demands a standardized and structured interface for tool discovery, invocation, and response handling. The model context protocol (MCP) [14] addresses this need by defining a formal client-server architecture that connects LLM hosts to external tools and services through well-defined schemas and execution semantics. By decoupling reasoning from execution, MCP provides a unifying protocol for intelligent, model-driven interaction with diverse and distributed technical environments.

LLM-based agents have already been widely adopted in domains such as software engineering [15] (e.g., repository management, issue tracking), personal productivity [16] (e.g., calendar scheduling, daily task automation), and data analytics [17] (e.g., structured knowledge base querying). More recently, tool-augmented or MCP-enabled LLM systems have been expanded and applied to a broader range of applications, including communication and edge computing systems [18], Internet-of-Things networks [19], electronic design automation [20], and photonic integrated circuits design [21]. These developments demonstrate the growing role of LLM agents as orchestration layers that bridge natural language intent and structured system interfaces.

Within networking and optical systems, LLM-based agents have been explored for monitoring, diagnosis, control, and performance optimization [22]–[25]. In most approaches involving device control, the agent translates user requests—often combined with device manuals, schema definitions, or reference code—into executable control scripts or structured SDN API calls. This workflow, illustrated in Fig. 1(b), relies on the LLM to synthesize control logic that directly interfaces with device APIs or controller northbound interfaces. While such code-generation or API-synthesis approaches reduce manual scripting effort, they remain tightly coupled to textual reasoning and prompt conditioning. At the level of individual hardware components, significant challenges persist, particularly in ensuring high-fidelity tool invocation, strict parameter validation, and robust handling of dynamic or ambiguous user inputs across heterogeneous devices. These limitations motivate the need for a more structured abstraction layer between LLM reasoning and physical device execution.

In this paper, we present AgentOptics for autonomous, scalable, and high-fidelity optical device control built upon MCP. As shown in Fig. 1(c), AgentOptics introduces a standardized and structured abstraction layer that leverages LLM-based reasoning to translate user natural language inputs into protocol-compliant operations, invoking corresponding MCP tools across heterogeneous optical devices through validated API calls. We implement 64 standardized MCP tools spanning eight representative optical devices (see Table I), encapsulating common device operations as deterministic, executable primitives. By exposing device operations through structured MCP-based tool schemas and leveraging LLMs, AgentOptics enables dynamic workflow orchestration without requiring task-specific code generation.

To systematically validate and evaluate the performance of AgentOptics, we construct a benchmark consisting of 410 tasks executed on real hardware and systems, covering single-, dual-, and triple-action invocations across multiple devices. The benchmark also includes five representative task variants, including *paraphrasing*, *non-sequitur*, *error*, *roles*, and *chain*, designed to emulate realistic and diverse user inputs

to assess the robustness and fidelity of AgentOptics under dynamic interaction scenarios. We implement AgentOptics using five representative commercial online LLMs, including GPT, Claude, and DeepSeek, as well as three locally deployed open-source models of varying parameter sizes. For comparison, we establish an LLM-based code generation (CodeGen) baseline with two variants: (i) online LLM-based optical device control via direct code generation, conditioned on either device manuals or reference control code, and (ii) a locally deployed LLM fine-tuned on optical device control code using low-rank adaptation (LoRA).

Overall, AgentOptics achieves an average success rate of 99.0% with online LLMs and 87.7% with locally deployed models across 410 benchmark tasks. In contrast, the CodeGen baseline attains average success rates of up to only 50.0%. AgentOptics enables practical natural language control of optical devices, achieving 98.1%–99.8% success rates with online LLMs at a token cost ranging from \$0.004 to \$0.15 per task, while locally deployed models achieve 87.1%–88.8% success rates at near-zero cost per task.

We further demonstrate the capabilities of AgentOptics through five representative case studies: (i) In a ROADM-based dense wavelength-division multiplexing (DWDM) network, AgentOptics provisions a coherent 400 GbE signal alongside an analog radio-over-fiber (ARoF) signal and performs coordinated multi-device monitoring of link performance metrics, including optical signal-to-noise ratio (OSNR) and error vector magnitude (EVM). (ii) For a wideband ARoF link carrying 5G fronthaul traffic, AgentOptics autonomously characterizes system performance and optimizes the ARoF transmitter bias voltage to enhance wireless transmission quality. (iii) In a two-span link with co-propagating comb channels, AgentOptics provisions additional 400 GbE channels and autonomously adjusts launch power to minimize the pre-forward error correction (pre-FEC) bit error rate (BER). (iv) For polarization-sensitive links, AgentOptics enables closed-loop polarization stabilization through orchestrated measurement and actuation, maintaining convergence despite intentional fiber perturbations. (v) For distributed acoustic sensing (DAS)-based fiber sensing systems, AgentOptics automates sensing operations, data acquisition, and LLM reasoning to identify potential fiber cut events. The AgentOptics implementation and benchmark are open-sourced at [26].

This paper is organized as follows. We review the background and related work in Section II, and describe the proposed system architecture and implementation in Section III. Sections IV and V present the benchmarking methodology and experimental results. We demonstrate practical capabilities of AgentOptics through five case studies in Section VI, and conclude in Section VII.

II. RELATED WORK

A. Agentic AI Frameworks and Applications

Unlike traditional AI systems that generate single-shot text responses, agentic AI extends LLMs to perform goal setting, multi-step planning, external tool interaction, and feedback-driven decision-making. A defining feature of such agents

is their ability to act on external systems, typically through structured tool function calling. There are multiple methods through which an LLM may invoke a tool function: the tool name and definition may be (i) implicitly acquired during pre-training [27], which requires massive training data; (ii) provided as part of the input prompt and executed via an external controller [28], where the context length linearly with tool count; (iii) accessed through a specific protocol such as MCP [14], which provides a standardized schema but adds protocol overhead; or (iv) implemented via program-aided language (PAL) models [29], where the model directly generates executable control code, which offers flexibility but lacks safety validation.

These methods enable LLMs to interact with a wide range of real-world applications. For example, HuggingGPT [30] is an early example that uses an LLM as a controller to route user requests to specialized expert models and aggregate their output into a comprehensive response. SWE-agent [15] demonstrates a repository-level automation agent for software engineering. IoT-MCP [19] bridges LLMs and heterogeneous devices for IoT system development. In scientific reasoning and verification, ax-Prover [31] shows the agent’s capability in theorem proving for mathematics and quantum physics. Similarly, physics Supernova [32] demonstrates near-gold medal performance on International Physics Olympiad problems. Seed-Prover [33] reaches undergraduate- to PhD-level mathematics capability. In addition, a multi-agent framework achieves single-device design [21]. In the broader networking area, agentic pipelines have been explored for intent-based infrastructure and service orchestration [34], as well as wireless and O-RAN management [35].

B. Agentic AI in Optical Network Monitor and Control

In optical networks, recent LLM-based systems began to couple language-guided decision making with operational interfaces, enabling workflows that interpret telemetry and logs, coordinate control-plane actions, and verify outcomes through feedback from the network and devices.

Agentic optical network diagnosis and monitoring. Several studies have applied LLM agents to optical network diagnosis and monitoring tasks, primarily focusing on analytical reasoning and decision support. In [36], a GPT-4-powered agent was proposed to support autonomous optical network management, such as quality of transmission (QoT) estimation, performance analysis, optimization, and calibration. AlarmGPT [22] in a LangChain-based tool-augmented workflow that automates optical transport networks for alarm interpretation, compression, prioritization, and diagnosis. [23] presented an instruction-tuned LLM for field-collected optical network log parsing, anomaly detection and classification, and report generation.

Agentic optical network control. Recent works have also explored LLM-based automation for optical network control [37]. These approaches typically employ external grammars to convert natural language outputs into valid executable instructions, incorporate device API descriptions through prompt engineering, or fine-tune models to directly generate structured function calls. For example, [38] proposed

an LLM-driven pipeline that leverages formal grammars to constrain the LLM output to valid JSON-formatted device control instructions for SDN configuration. Another approach to instruction generation is embedding device API specifications directly within prompts, and it was demonstrated in [25] that amplifier gain optimization can be performed via SDN API in prompts. Similarly, AutoLight presented in [24] is a multi-agent framework for distributed AI training using optical communications API as LLM input reference. Finally, smaller LLMs fine-tuned on network-specific control instructions have been used to directly generate executable commands [39].

However, existing LLM-based autonomous device and network control methods introduce three major limitations. First, these approaches assume the existence of a mature SDN infrastructure with an external instruction-formatted grammar. Changes to the SDN infrastructure typically require reconstruction or substantial modification of the grammar and LLM-related control mechanisms. Second, in large-scale networks with multi-vendor devices, the number of tools and associated function descriptions grows significantly. This results in lengthy prompts containing extensive tool specifications for each function call or agent invocation, leading to increased token consumption and higher operational costs. Finally, the fine-tuning process itself presents additional challenges. Each SDN adaptation requires a dedicated dataset of user requests paired with appropriate SDN tool calls. Consequently, whenever new devices or vendors are added, further adaptation and re-training of the LLM are necessary. In addition, fine-tuning often leads to overfitting, as demonstrated in our manuscript by the baseline of local LLM-based code generation. The fine-tuned model performs well when user inputs closely match the distribution of the request–tool training dataset; however, when users paraphrase their requests, the task execution success rate declines significantly. This sensitivity to linguistic variation limits the robustness and practical applicability of such methods.

To address these limitations, AgentOptics adopts a protocol-centric design that fundamentally separates language reasoning from device execution. Rather than relying on handcrafted grammars or embedding detailed tool specifications directly into the prompts—which become unscalable in evolving, multi-vendor infrastructures—AgentOptics introduces a structured protocol-level interface that standardizes tool invocation independent of natural language phrasing. This decoupling eliminates the need for continual grammar updates as devices or APIs change. Moreover, by abstracting execution into a protocol-governed layer instead of fine-tuning on request–tool pairs, AgentOptics better preserves the native reasoning capabilities of LLMs and enables reliable closed-loop automation across heterogeneous devices.

III. AGENTOPTICS: DESIGN AND IMPLEMENTATION

In this section, we present the design and implementation of the AgentOptics for optical device control built on MCP, comprising 64 MCP tools across eight representative optical devices and supporting both cloud-hosted commercial and locally deployed open-source LLMs.

A. MCP-based Agentic System Design

MCP is an open and standardized interoperability protocol designed to enable structured communication between LLM-based applications and external data sources, tools, and services. It defines a formal client-server architecture in which the MCP client typically resides on the user side, while MCP servers are deployed on the device side, allowing LLM hosts to systematically discover, access, and utilize contextual resources exposed by devices. In AgentOptics, as illustrated in Fig. 1(c), a user initiates interaction by issuing a natural language task (e.g., querying the status of an EDFA), which is received by an MCP client embedded within the host application. The client forwards the task to the LLM, which interprets the user intent using domain knowledge and selects the relevant and appropriate MCP server(s) based on its published server description. Subsequently, the client retrieves the available tool descriptions and function definitions from the selected MCP server(s) and supplies them to the LLM, which determines the most suitable tool by evaluating semantic similarity between the user task and tool metadata. The selected tool is then executed by the MCP server, invoking device-specific APIs, monitoring task completion, and returning the execution results to the MCP client. Finally, the MCP client relays the results back to the LLM, which processes the output and generates a human-readable natural language response for the user. Note that the LLM interacting with the MCP client can be either an online commercial model (e.g., GPT-5 or Claude Sonnet 4.5) or a locally deployed open-source model (e.g., Qwen-14B) with fine-tuning if needed, depending on considerations such as performance, cost, latency, and privacy, which are evaluated in Sections IV and V.

This MCP-based design offers several advantages for agentic AI-based optical device control compared with existing approaches [25], [39]. First, each MCP tool encapsulates a well-defined operational capability, allowing the MCP client to invoke device functions without granting the LLM direct access to low-level device systems or requiring it to generate control code, thereby enhancing robustness and operational safety. Second, the decoupled implementation of MCP clients and servers enables remote device operation across network boundaries, providing increased flexibility in system deployment and access control. For example, a user can run the MCP client on a separate host while keeping the MCP server close to the optical devices, so multi-device actions (e.g., configuring ROADM channels and then measuring spectrum from OSA) are executed locally, and only the structured results are returned to the client. Finally, MCP provides a uniform communication interface that abstracts vendor-specific protocols, enabling administrators and users to operate systems composed of diverse optical hardware through the same tool interface, even when the underlying devices use different control protocols, without necessitating retraining or fine-tuning of the underlying language models.

B. Implementation of MCP Servers and Tools

We implement eight MCP servers for eight representative optical devices, as summarized in Table I: (i) Lumen-

Optical Device	# of Tools	Example Tools
Lumentum ROADM	10	Set/get EDFA gain; set/get WSS connections/attenuation, ...
Lumentum 400 GbE CFP2-DCO	6	Set center frequency/output power/operation mode; get config, ...
OptiLab LT-12-EM ARoF TX	6	Set bias voltage/current; get status, ...
APEX Technologies OSA	26	Get power/spectrum; set/get measurement parameters, ...
Calient S320 Optical Circuit Switch	4	Get port; add/delete connection; delete all connection
DiCon MEMS 32×32 Optical Switch	2	Get connections; set connection
Luna POD2000 Polarimeter	7	Set configuration; read polarization, read power, ...
Luna PCD-M02 Polarization Controller	3	Reset DAC code; set DAC code; set voltage

TABLE I: List of optical devices and validated MCP tools supported by AgentOptics.

tum ROADM including booster/preamp erbium-doped fiber amplifiers (EDFAs) and 1×20 MUX/DEMUX WSSs; (ii) Lumentum 400 GbE CFP2-DCO tunable TRX; (iii) Optilab analog radio-over-fiber (ARoF) transmitter (TX) based on electro-absorption modulator (EAM); (iv) APEX Technologies optical spectrum analyzer (OSA); (v) Calient S320 optical circuit switch (OCS); (vi) DiCon MEMS 32×32 optical switching system; (vii) Luna POD2000 polarimeter; and (viii) Luna PCD-M02 miniature multi-channel piezoelectric actuator driver card with integrated PolarITE III polarization controller. For each device, we implement its respective MCP server that exposes a set of tools supporting core operations, including device setup, parameter control, status monitoring, and connection reconfiguration. Note that one tool list above can include many smaller tools, and we implement our tools based on our needs. The design architecture of AgentOptics is inherently extensible to a broad range of optical devices and instruments, enabling the construction of scalable systems composed of heterogeneous components.

We implement AgentOptics interacting with two types of LLM serving for optical device control: online commercial LLMs and locally deployed open-source LLMs:

- **MCP with online LLM (AgentOptics-Online)**, where the MCP client sends tasks to online LLMs. We consider various online models from different platforms¹, including GPT-4o mini, GPT-5, Deepseek-V3, Claude Haiku 3.5, and Claude Sonnet 4.5. GPT-4o mini and DeepSeek-V3 have the lowest input costs (\$0.15/\$0.6 and \$0.28/\$1.1 per 1M input/output tokens, respectively), favoring high-frequency, long-context usage, while Haiku 3.5 and Sonnet 4.5 are more expensive (\$1/\$5 and \$3/\$15 per 1M input/output tokens, respectively) due to their larger model capacity. GPT-5 occupies an intermediate position with a cost of \$1.25/\$10 per 1M input/output tokens, balancing computational cost and reasoning performance.
- **MCP with local LLMs (AgentOptics-Local)**, which are hosted on a local Dell PowerEdge R750 server with a 64-core Intel Xeon Gold 6548N CPU @2.6 GHz and a NVIDIA 40GB A100 GPU. Qwen models with parameter sizes of 0.4B, 8B, and 12B are selected. All models are deployed without quantization using the vLLM inference framework. Unlike online commercial models, locally deployed LLMs incur no per-token usage costs; instead, expenses are dominated by electricity

¹Model pricing is based on publicly available rates as of February 2026.

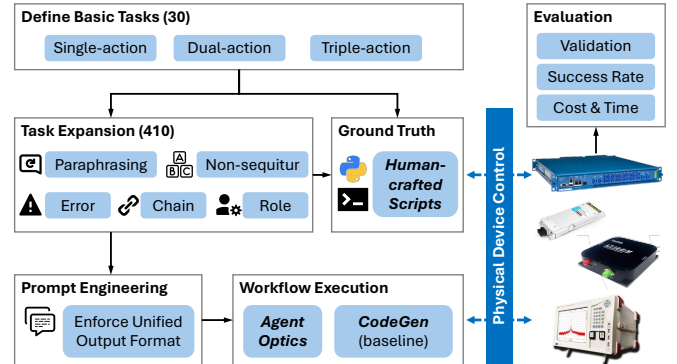


Fig. 2: Benchmark workflow for evaluating the performance of AgentOptics and the CodeGen baseline, where reference ground truth is established using human-crafted scripts that are manually validated on physical devices for correctness.

consumption and one-time investments in GPU and server hardware. Consequently, the effective token cost of local LLM inference is considered negligible and approximated as zero in our analysis.

IV. EXPERIMENTAL EVALUATION

We compare two workflows for operating real optical devices from natural language task descriptions: (i) AgentOptics, and (ii) an LLM-based code generation approach (CodeGen), both within a carefully crafted evaluation benchmark.

A. Evaluation Benchmark

As shown in Fig. 2, the evaluation benchmark begins basic operational tasks, categorized into single-, dual-, and triple-action tasks. Each task corresponds to one or more optical device action requests, such as reading device status or configuring operational parameters, expressed in human-readable language. These tasks are then translated into structured action sequences for execution and evaluation, where prompt engineering is also applied to enforce a unified output format, enabling consistent downstream processing. We implement device control scripts based on manufacturer manuals and existing codebase to obtain the **ground truth** device status and operation results (see Fig. 1(a)), which provides the most accurate and reliable reference for validating optical device operations, and has been extensively used and validated across a series of works [4], [40]–[45]. For example, the ROADM control scripts have been used for collecting EDFA gain profile datasets [40], as well as modeling and optimizing multi-span

link quality of transmission [46]–[48]. Similarly, the ARoF and OSA control scripts have been used to study the coexistence of fiber sensing, 400 GbE, and 5G signals in field trials [49].

To evaluate the performance of AgentOptics, each benchmarking task is executed on real optical devices and compared with the ground truth. All workflows run within an identical execution environment, ensuring controlled and reproducible comparisons. We consider *task success rate* as the primary metric, where the task is labeled as success when the hardware behavior results based on the task execution match the expected device behavior results. More specifically, this includes: (i) correct tools and invocation order; (ii) correct arguments used for tool invocation; and (iii) execution results meet task intents. We use DeepSeek-V3 to analyze execution result logs, enabling reasoning about the root causes of the failed tasks to identify execution errors.

We also consider the *average cost* per task by multiplying the token consumption of each task execution by the corresponding per-token prices of different online LLMs. For locally deployed open-source LLMs, the per-token cost is effectively negligible, with expenses dominated by electricity consumption and one-time investments in server and GPU hardware. Therefore, the per-task cost for local models is approximated as zero in our evaluation. Moreover, we record the *execution time* per task, including the time spent on task input, tool selection, device control, and retrieval and analysis of the returned value. For tasks involving multiple actions, the execution time is measured as the total time required to complete all actions.

B. Agentic Optical Device Control Tasks

To systematically evaluate the performance of AgentOptics, we develop a benchmark consisting of a comprehensive set of carefully designed user tasks, as shown in Fig. 2. The benchmark evaluates agent performance across multiple dimensions, including the number of device-control APIs required to execute a user command, robustness to diverse natural language inputs, error-handling capability, and support for multi-vendor device operation and coordination. This benchmark spans a representative set of optical hardware, including a Lumentum ROADM, a 400 GbE coherent CFP2-DCO, an OptiLab ARoF transmitter, and an APEX OSA, which are commonly used together across a wider range of optical networking and experimentation workflows. The benchmark includes user tasks that involve one to three actions (e.g., invoking vendor-specific APIs) spanning multiple devices. For example, a single-action task may read the signal spectrum from an OSA, while a dual-action task may combine two related or unrelated operations within a single prompt, such as reading signal spectrum from an OSA followed by setting the output power of an EDFA.

We further extend each task to multiple representative variants, designed to evaluate the robustness of the agentic AI framework under conditions commonly encountered in day-to-day optical device and network control. Specifically, we consider five types of *task variants* (Table II):

- **Paraphrasing** evaluates semantic understanding by testing whether the agent can recognize differently worded

instructions with identical intent (e.g., “OSA measure” \Leftrightarrow “OSA data recording”);

- **Non-Sequitur** assesses robustness to irrelevant or incoherent instructions that should not result in valid actions (e.g., “OSA measure, watch TV”);
- **Error** tests the agent’s ability to detect and reject invalid or unsafe commands (e.g., “Set OSA wavelength to 0”);
- **Chain** measures multi-step reasoning and state consistency across sequentially dependent commands (e.g., “Set EDFA gain, then read EDFA gain”);
- **Role** evaluates contextual and role-based instruction following, where task execution depends on an assigned role (e.g., “Act as the service provider, OSA measure”).

The benchmark begins with 30 basic tasks—10 single-action, 10 dual-action, and 10 triple-action, which are systematically expanded into a total number of 410 tasks spanning multiple difficulty levels. Specifically, for each basic *single-action* task, we generate five paraphrasing variants and five non-sequitur variants, as well as three error variants and three role-conditioned variants, yielding $10 \times (5 + 5 + 3 + 3) = 160$ expanded tasks. The error and role-conditioned variants are restricted to single-action tasks because their localized decision point allows controlled error and role-conditioned modifications without altering task semantics; in multi-action tasks, such modifications would propagate ambiguously across independent steps. For each basic *dual-action* task, we generate five paraphrasing variants and five non-sequitur variants, as well as 10 chained variants constructed by converting the two-step format into a single sequential instruction that includes both steps (e.g., “(1) set ...; (2) get/read ...” \Rightarrow “set ... and then get/read ...”), each with five paraphrasing variants, yielding $10 \times (5 + 5) + 10 \times 5 = 150$ expanded tasks. For each basic *triple-action* task, we generate five paraphrasing variants and five non-sequitur variants, yielding $10 \times (5 + 5) = 100$ expanded tasks. In total, this yields 410 expanded tasks that are used for evaluating the performance of AgentOptics.

C. Baseline: LLM-based Code Generation (CodeGen)

We evaluate AgentOptics against LLM code generation workflows that rely on either user manuals provided by the device manufacturer or pre-existing code libraries for direct device operation, as illustrated in Fig. 1(b). The code generated by LLM is then executed in a clean and isolated runtime environment, which uses the generated code to execute on actual devices. The return output and execution logs/errors from the device are captured for evaluation. The task success rate for the CodeGen baseline is defined identically to that for AgentOptics described in Section IV-A, where only the hardware returned results that meet the expectation is considered as success. We evaluate both online high-capacity models and a locally hosted model supporting privacy-preserving deployments:

- **LLM-based code generation with online LLMs (CodeGen-Online)**. This baseline uses online LLMs (e.g., Claude Sonnet 4.5) to generate control code in Python based on the device documentation. The LLM

Type	Description	Task example
Paraphrasing	Same meaning, different phrases	<ul style="list-style-type: none"> Operate the CFP2 so that port cfp2-opt-1-1 has an output target power setting of -5 dBm. Using the CFP2, adjust the output target power parameter on port cfp2-opt-1-1 to -5 dBm.
Non-sequitur	Adding unrelated information to the task	<ul style="list-style-type: none"> Set CFP port cfp2-opt-1-1 power to -5 dBm; the bench mat has a curled corner.
Error	Task with wrong or lost value	<ul style="list-style-type: none"> Missing power value: on the CFP2, set output target power on port cfp2-opt-1-1. Wrong power value: on the CFP2, set output target power on port cfp2-opt-1-1 to -100 dBm.
Chain	Sequential related tasks	<ul style="list-style-type: none"> First set CFP2 port cfp2-opt-1-1 output target power to -4 dBm, then read CFP2 output power.
Roles	Task tone as service provider or user	<ul style="list-style-type: none"> You are an optical device user; set CFP port cfp2-opt-1-1 power to -5 dBm.

TABLE II: Five representative task variants evaluated in the agentic optical device control benchmark.

receives task descriptions, device connection information (e.g., IP address, serial ports, USB identifiers), and relevant materials in one of the two forms: (i) vendor-provided manuals, including APIs/code that is part of the manual (CodeGen-Online with manual), or (ii) reference code libraries for each target device (CodeGen-Online with code). The LLM then produces executable code to control the target optical devices.

- LLM-based code generation with local LLMs (CodeGen-Local):** This baseline uses CodeLlama-7b-hf [50], which is a 7 billion-parameter foundation model in the Code Llama family developed for general code synthesis and understanding, capable of generating programming code from natural language or partial code prompts. However, small local models such as CodeLlama-7b-hf usually exhibit significantly weaker code generation performance compared to online models. To mitigate this limitation, we applied low-rank adaptation (LoRA) fine-tuning [51] using a local dataset consisting of user-issued device control commands (e.g., requesting an OSA spectrum measurement) paired with their corresponding control code. This task-specific adaptation transforms a general-purpose local LLM into a specialized optical device control model, substantially improving control accuracy and execution success rates. The LoRA fine-tuning employs a learning rate of 3×10^{-4} over 100 epochs.

V. RESULTS

We evaluate the performance of AgentOptics using different online commercial and local-deployed open-source LLMs under the benchmark described in Section IV, compare AgentOptics against CodeGen baselines, analyze agentic AI execution error types, and finally compare the cost and execution time of AgentOptics with the CodeGen baseline.

A. AgentOptics with Online and Local LLMs

Fig. 3 shows the success rate achieved by AgentOptics for tasks with varying numbers of actions under different online (AgentOptics-Online) and local (AgentOptics-Local) LLMs. Overall, online commercial models (e.g., GPT-4o mini, Claude Sonnet 4.5, and DeepSeek-V3) achieve average success rates of 95.6%–99.4% for single-action tasks, 99.3%–100.0% dual-action tasks, and 97.0%–100.0% for triple-action tasks. In

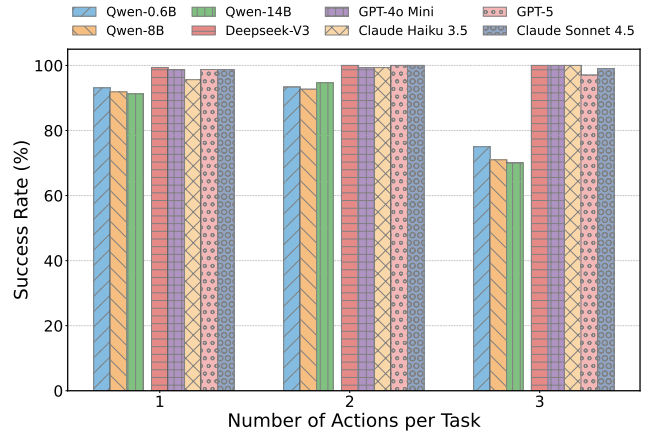


Fig. 3: Task success rate achieved by AgentOptics across varying task complexities using three locally hosted and five online LLMs.

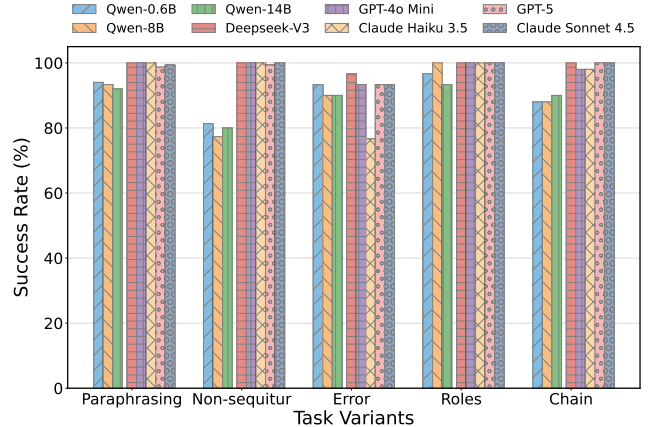


Fig. 4: Task success rate achieved by AgentOptics across different task variants using three locally hosted and five online LLMs.

contrast, open-source locally deployed models (e.g., Qwen-0.6B and Qwen-14B) exhibit a noticeable degradation in performance, particularly when more actions are involved in the task: their success rates drop from 91.3%–93.1% for single-action tasks and 92.7%–94.7% for dual-action tasks to 70.0%–75.0% for triple-action tasks, highlighting the impact of model capacity on multi-tool coordination reliability. Notably, model performance is also affected by how an LLM is trained to support MCP. For example, GPT-4o mini, despite having much fewer parameters than GPT-5, demonstrates consistently strong performance across all tasks.

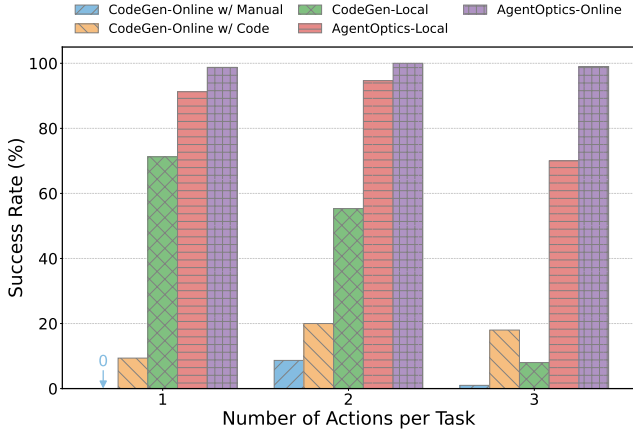


Fig. 5: Task success rate achieved by AgentOptics across varying task complexities using locally hosted and online LLMs, and comparison to the CodeGen baseline that leverages LLM for code generation.

Fig. 4 shows the success rate achieved by AgentOptics across different task variants described in Section IV-A (see also Table II). Overall, all evaluated models perform well on the paraphrasing (92.0%–100.0%) and role (93.3%–100.0%) variants, indicating strong robustness to linguistic reformulation and role-based prompt conditioning. In contrast, the performance of AgentOptics degrades for more challenging task variants such as non-sequitur and error detection. For the non-sequitur variant, commercial online models (e.g., GPT-5, Claude Sonnet 4.5, and DeepSeek-V3) achieve success rates between 99.3% and 100.0%, whereas locally deployed LLMs achieve only 77.3%–81.3%, often failing to select the appropriate tool when user prompts contain unrelated or extraneous information. The error variant poses challenges for both online and local models: online models achieve success rates ranging from 76.7% (Claude Haiku 3.5) to 96.7% (DeepSeek-V3), while local models achieve 90.0%–93.3%. Although explicit error-handling mechanisms are implemented within the MCP tools integrated in AgentOptics, missing or incomplete input parameters can still cause LLMs to invoke incorrect APIs or tools, e.g., calling a configuration setting function as a read operation due to the absence of required tool invocation parameters.

B. AgentOptics and CodeGen Performance Comparison

Next, we compare the performance of AgentOptics against the CodeGen baseline using both an online model (Claude Sonnet 4.5) and a locally deployed, domain fine-tuned model (CodeLlama-7b-hf, see Section IV-C). Fig. 5 shows the corresponding task success rates for single-, dual-, and triple-action tasks, where AgentOptics consistently achieves the highest success rates across all task complexities. In particular, AgentOptics-Online attains near-perfect performance, achieving success rates of 98.8%–100.0%. On the other hand, the CodeGen baseline exhibits substantially lower success rates across all task complexities. Notably, CodeGen-Local shows a clear degradation as the number of required actions increases (71.3% → 55.3% → 8.0%). For example, on single-action tasks, CodeGen-Local achieves a success rate of 71.3%,

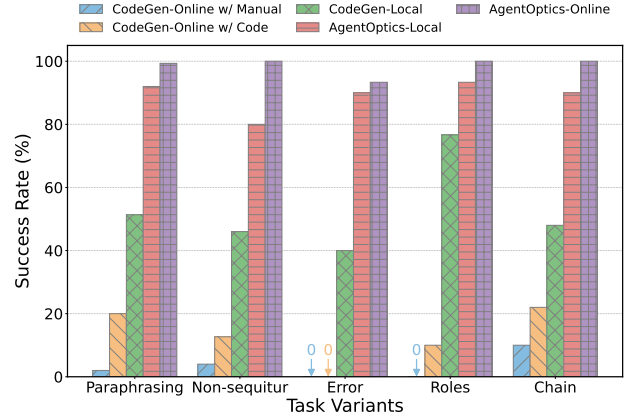


Fig. 6: Task success rate achieved by AgentOptics across different task variants using locally hosted and online LLMs, and comparison to the CodeGen baseline that leverages LLM for code generation.

whereas AgentOptics-Online maintains a success rate of 98.8%. This performance gap is more significant for complex tasks: for triple-action tasks, CodeGen-Local achieves a success rate of only 8.0%, whereas AgentOptics-Online maintains a success rate of 99.0%. Notably, CodeGen-Online with code and manuals performs even worse—achieving success rates of at most 20.0%—due to the lack of domain-specific knowledge in the online model. In contrast, CodeGen-Local outperforms the CodeGen-Online variants on low-complexity tasks (e.g., 71.3% vs. 9.4% for single-action tasks), primarily due to the benefits of LoRA fine-tuning. However, this advantage comes at the expense of scalability, as the local LLM must be fine-tuned every time with new devices or features.

Fig. 6 reports the success rate across different task variants, including paraphrasing, non-sequitur, error, role, and chain. AgentOptics leveraging MCP consistently outperforms the CodeGen baseline across all variants, with AgentOptics-Online achieving 93.3%–100.0% across all task types. In contrast, the CodeGen baseline exhibits substantially lower performance, particularly under more challenging variants such as error induced (0.0% for both CodeGen-Online variants vs. 93.3% for AgentOptics-Online) and chain tasks (22.0% for CodeGen-Online with code vs. 100.0% for AgentOptics-Online). CodeGen-Local achieves superior performance compared to CodeGen-Online with code (e.g., 51.3% vs. 20.0% success rates on paraphrasing tasks), benefiting from LoRA fine-tuning. Moreover, providing reference code has a higher success rate than providing a user manual.

C. Cost Efficiency and Execution Time

Fig. 7 shows the trade-offs between task success rate and average cost (\$/task) achieved by AgentOptics and the CodeGen baseline for dual-action tasks with different LLMs. Online commercial LLMs show a wide range of (*cost, success rate*) performance: high-end online models such as GPT-5 (\$0.048/task, 98.8%) and Claude Sonnet 4.5 (\$0.152/task, 99.3%) achieve high success rate at substantially higher cost, whereas lightweight online models such as GPT-4o mini (\$0.004/task, 99.3%) and DeepSeek-V3 (\$0.011/task, 99.8%)

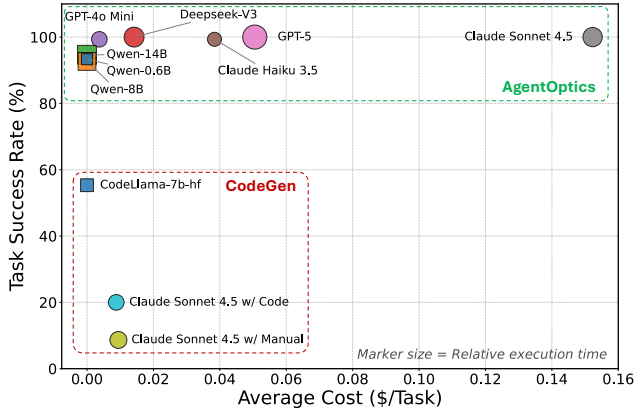


Fig. 7: Trade-off between success rate and average cost for dual-action tasks with AgentOptics and the CodeGen baseline using locally hosted (squares) and online (circles) LLMs. Marker size indicates the relative average execution time.

achieve the best performance at significantly lower cost—both match or exceed the success rate achieved by more expensive models. Locally deployed models such as Qwen-14B provide competitive (87.3%) accuracy at minimal cost. In contrast, the CodeGen baseline exhibits both limited accuracy (e.g., only up to 50%) and cost efficiency. Notably, AgentOptics is not cost-efficient when paired with high-cost models such as Claude Sonnet 4.5, even compared to both CodeGen-Online variants with code and manuals (\$0.010/task), which itself requires providing extensive device manuals—often tens to hundreds of pages—or reference codebases consisting of hundreds to thousands of lines of code. For example, AgentOptics using Claude Sonnet 4.5 and GPT-4o mini achieve identical task success rates, yet the latter incurs a $38\times$ lower cost per task, suggesting that for specific applications, higher-cost models provide negligible improvements in success rates relative to their substantially increased cost.

We also report the relative execution time of different methods in Fig. 7, indicated by the size of the circles. On average, for AgentOptics, execution time varies significantly across models. Higher-capacity, reasoning-oriented models (e.g., GPT-5 at 23.8 sec, Claude Sonnet 4.5 at 13.1 sec, and DeepSeek-V3 at 16.4 sec) show longer runtimes compared to smaller models optimized for throughput (e.g., Qwen-0.6B at 4.0 sec, GPT-4o mini at 11.3 sec). When comparing AgentOptics with the CodeGen baseline using the same LLM (e.g., Claude Sonnet 4.5), AgentOptics incurs additional latency (11.4 sec vs. 8.6 sec for CodeGen-Online-Code) due to potentially multiple rounds of communication between the client and LLM running the MCP-based method.

D. Agentic AI Execution Error Types

To understand the remaining failures under this benchmark, Table III summarizes common failure modes observed when applying AgentOptics and the CodeGen baseline. For CodeGen, failures primarily stem from software-level issues, including importing non-existent libraries, invoking invalid functions or class attributes, and generating syntactically incorrect code. For example, the prompt with “set the target output

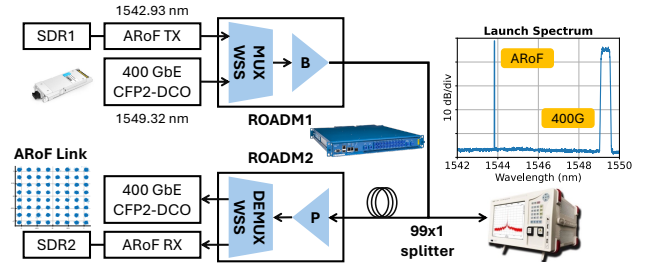


Fig. 8: Diagram for DWDM link with ARoF and 400 GbE signals.

power of a CFP2 module to -5 dBm” leads to the error “*ERROR: CFP2 object has no attribute set_output_power*”. Such errors indicate limitations in CodeGen’s ability to accurately reason about programming language syntax and library semantics under complex task requirements. In contrast, AgentOptics failures are mainly related to tool orchestration, such as missing required tool invocations, incorrect tool naming due to formatting inconsistencies, calling undefined MCP tools, or executing on only a subset of the tools necessary to complete a task. For example, “Set the OSA start wavelength to 1545 nm” which requires calling the tool `osa_set_start_wavelength`, but AgentOptics actually invokes the tool `osa_set_center_wavelength`. These failure modes suggest that while AgentOptics can often reason correctly about individual tools, it still struggles with reliably coordinating multiple tools.

VI. CASE STUDIES

AgentOptics is not limited to high-fidelity control of individual optical devices under diverse natural-language inputs, but also extends to more comprehensive network production scenarios, including optical link configuration, autonomous channel QoT optimization, quantum polarization control, and automatic fiber cut event detection. We demonstrate these capabilities through four representative case studies.

A. DWDM Link Setup and Performance Monitoring

To evaluate the AgentOptics capability to coordinate multi-vendor multi-device optical network operation, we establish a DWDM link that integrates Lumentum ROADMs with coherent 400 GbE and ARoF subsystems. This configuration, shown in Fig. 8, demonstrates end-to-end wavelength provisioning with coordinated control across multiple signal types. The topology consists of two ROADM units (ROADM1 and ROADM2) interconnected through a 99×1 optical splitter, where the 1% port is directed to an OSA for real-time monitoring while 99% of the optical power propagates through a 20 km fiber spool connected to ROADM2. Each ROADM unit includes both MUX/DEMUX WSS modules as well as booster (B) and pre-amplifier (P) EDFAs. In this experiment, we configure only the required subset of the components, using the MUX WSS and booster EDFA on ROADM1 and the DEMUX WSS and pre-amplifier EDFA on ROADM2. This architecture enables wavelength routing with optical amplification for span loss compensation.

Methods	Failure Category	Example Description
CodeGen	Import non-existing library	Imports an undefined library (e.g., <code>import lab_api</code> which is undefined).
CodeGen	Call non-existing function	Calls an invalid function (e.g., <code>call AP2XXX.get_powower</code> which is not existed).
CodeGen	Syntax error	Contains invalid syntax (e.g., <code>IP=' '192.168.0.2</code>).
AgentOptics	Missing tool	Required tools are not invoked (expected OSA-related tools, but called none).
AgentOptics	Incorrect tool	Call the wrong tool (e.g., <code>arof_get_power</code> \leftrightarrow <code>arof_read_power</code>).
AgentOptics	Calling non-existent tool	Invokes an undefined MCP tool (e.g., <code>cfp2_get_voltage</code> which does not exist).

TABLE III: Reasons and examples for CodeGen and MCP-based AgentOptics execution failures.

Using an agentic workflow, AgentOptics executes a coordinated multi-device control sequence from an operator intent to provision the two optical channels described below. In this case study, the agent interacts with four devices (ROADMs, OSA, CFP2-DCO, and ARoF TX) and invokes a total number of nine tools. Note that although AgentOptics provides a spectrum measurement tool, it is not invoked here: high-resolution spectrum acquisition would require a large numerical array that significantly increases token consumption in the LLM context. Instead, the OSA tools here only configure the sweep window, and spectrum acquisition is performed outside the AgentOptics workflow. Specifically, it configure an ARoF path over 193.9–194.45 THz on port 1 and a CFP2 path over 193.4–193.7 THz on port 20 on both ROADMs, sets OSA sweep to 1540–1550 nm, sets the CFP2 center frequency to 193.5 THz, and applies 99 mA current and -0.9 V bias to the ARoF TX.

With these WSS paths and endpoints settings, the link carries two optical channels: an ARoF channel operating at 1542.92 nm (194.3 THz) for analog radio signal transmission and 400 GbE at 1549.32 nm (193.5 THz) by the CFP2-DCO for high-speed coherent data transmission. Both channels are routed through the ROADM WSS modules with appropriate power levels and port assignments. Performance monitoring successfully confirms provisioning with a measured OSNR of 32.6 dB for the 400 GbE signal by the CFP2-DCO and an error vector magnitude (EVM) of 3.91% for the ARoF signal, while the launch spectrum shows both channels at their designated wavelengths in Fig. 8.

B. Wideband 5G ARoF Link Characterization

In the second case study, we demonstrate AgentOptics controlling a wireless-optical testbed to autonomously characterize an initially unknown transmitter configuration. The experimental setup is shown in Fig. 9(a), where a radio frequency system-on-chip (RFSoc) ZCU216 board serves as the radio, generating and receiving a 400 MHz orthogonal frequency-division multiplexing (OFDM) signal centered at 600 MHz carrier frequency. We adopt the RFSoc implementation from [52] as the base hardware design, and the generated RF signal is subsequently modulated onto an optical carrier at 1552.44 nm (193.11 THz) using an Optilab LT-12-E-M EAM.

Within this framework, AgentOptics acts as the agentic control layer, dynamically configuring and sweeping the ARoF transmitter bias voltage while continuously measuring the ARoF link SNR and BER. Specifically, AgentOptics autonomously orchestrates the RFSoc ZCU216 board to transmit and receive 5G NR OFDM waveforms with different modulation schemes (QPSK, 16QAM, and 64QAM), using onboard signal processing to compute feedback metrics including SNR,

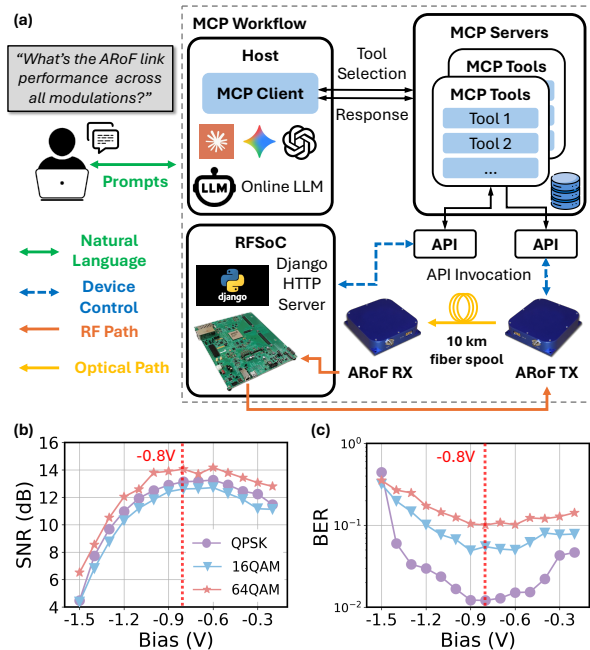


Fig. 9: (a) AgentOptics workflow for LLM-assisted wide-bandwidth ARoF 5G NR link with an RFSoc ZCU216 board and an ARoF transmitter-receiver pair. (b)–(c) Optimized ARoF transmitter bias voltage across link SNR and BER with different modulation orders.

EVM, and BER. The modulated ARoF signal is propagated over a 10 km fiber spool under varying ARoF transmitter bias voltages. Figs. 9(b)–(c) show the measured SNR and BER of the received OFDM signal across the automated ARoF link configurations. The results show that AgentOptics can characterize the ARoF link and, based on these measurements, identify and apply the optimal ARoF transmitter bias voltage for improved wireless transmission performance.

C. Adaptive Channel Configuration and GSNR Optimization on Multi-Span Optical Links

For the third case study, we demonstrate that AgentOptics is capable not only of basic link establishment but also of reasoning-driven operations such as channel power optimization. To illustrate this capability, we establish a two-span optical link consisting of two 400 GbE CFP2-DCO transceivers and an amplified spontaneous emission (ASE) comb source, as shown in Fig. 10. Specifically, ten ASE channels with 50 GHz channel spacing from 193.85–194.85 THz are injected at the first ROADM to emulate background traffic. At ROADM1, the WSS multiplexes the ASE channels and two 400 GbE signals from CFP2-DCOs, which are subsequently amplified by a booster EDFA and transmitted over a 20 km fiber spool.

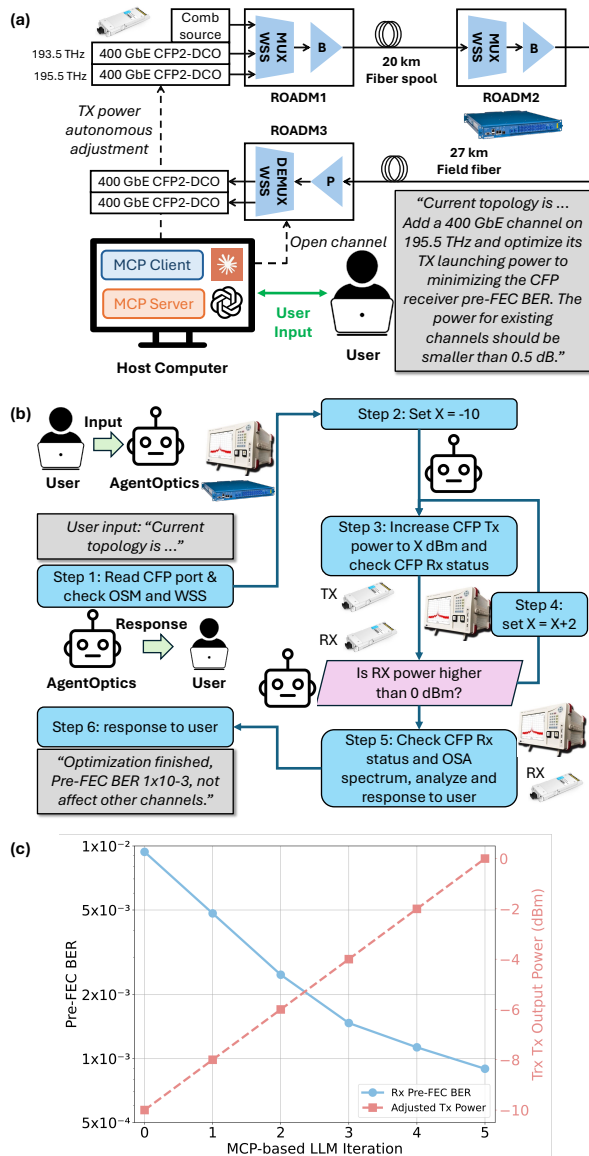


Fig. 10: (a) AgentOptics provisions a 400 GbE channel in a two-span link and autonomously optimizes the channel GSNR based on a single-line human language instruction. (b) Autonomous launch power optimization of the CFP2-DCO 400 GbE transmitter (TX) performed by AgentOptics. (c) Pre-FEC BER optimization of the 400 GbE signal by AgentOptics using an online LLM (Sonnet 4.5) without impacting existing background traffic.

The signals then pass through ROADM2 and subsequently propagate over a 27 km field fiber. Finally, the composite signal is amplified by a pre-amplifier and demultiplexed by the WSS in ROADM3, where the background ASE channels are dropped, and the two 400 GbE channels are directed to the receiver CFP2-DCO.

In this case study, we demonstrate AgentOptics’s capability for real-time dynamic link reconfiguration. Specifically, it adds a new 400 GbE channel centered at 195.5 THz using CFP2-DCO to the existing two-span link, and optimizes the transmitter launch power in order to minimize the pre-FEC bit error rate (BER) at the receiver to be below a given threshold. The user inputs link topology and reconfigura-

tion requirements, including channel adjustment constraints, minimal impact on existing channels, and 400 GbE channel optimization objectives, into the AgentOptics, as shown in Fig. 10(a). AgentOptics behavior during the channel power optimization is shown in Fig. 10(b), which is determined by AgentOptics itself. The user specifies the topology and optimization objective. In Step 1, the AgentOptics reads CFP port parameters and checks OSM and WSS status. In Step 2, the CFP Tx power is initialized to $X = -10$ dBm. In Step 3, the AgentOptics increases CFP Tx power to X dBm and queries CFP Tx/Rx status. A decision block evaluates whether CFP Rx power exceeds 0 dBm; if so, Step 4 updates the Tx power to $X + 2$ dB and repeats the loop. In Step 5, the AgentOptics analyzes CFP Rx status and OSA spectrum to verify pre-FEC BER and inter-channel impact. Finally, in Step 6, the agent reports the optimization results to the user, confirming minimized pre-FEC BER and negligible impact on existing channels.

The corresponding optimization results are shown in Fig. 10(c), where the x -axis denotes the iteration index as AgentOptics sequentially invokes different MCP tools to fulfill the user request for optimizing the BER for the newly added 400 GbE channel. A series of iterative steps are performed with a 2 dB step size to optimize the launch power of the CFP2-DCO, which is autonomously determined by the LLM (see Fig. 10(b), right y -axis). The left y -axis depicts the evolution of the pre-FEC BER of the newly added channel, demonstrating convergence to a minimized BER upon completion of the LLM-based optimization process. The optimization process automatically terminates once the CFP2-DCO receiver power reaches its predefined threshold.

D. Polarization Monitoring and Stabilization

The fourth case study demonstrates agentic control for automated polarization stabilization, which is crucial for a wide range of applications, including coherent optical communication [53], distributed interferometric fiber sensing [54], and polarization-sensitive quantum links such as entanglement-based quantum key distribution (QKD) [55]. Maintaining polarization stability is essential for fiber-optic links because environmental perturbation, such as temperature variation and vibration, can induce polarization drift over time and cause performance degradation. Traditionally, mitigating this drift requires researchers to manually activate polarization stabilization procedures upon observing degradation. In contrast, AgentOptics enables polarization correction through a single natural-language command, greatly simplifying operation and response time.

The experimental setup, as shown in Fig. 11(a), consists of a 1092 nm laser source, a Luna PCD-M02 4-channel piezo polarization controller, and a Luna POD2000 polarimeter. A host computer running an MCP client interfaces with an MCP server, which communicates with an Arduino Mega 2560 via USB. The Arduino device drives the PCD-M02 controller using 12-bit digital control codes (0–4095) via a digital-to-analog converter (DAC) interface; these codes map to an output voltage range from 0–5 V with a step size of

1.22 mV. In this case study, AgentOptics orchestrates two MCP-controlled devices—the POD2000 for polarization state measurement and the PCD-M02 (via Arduino) for actuation—and completes the workflow invoking four tools: configure the POD2000 wavelength (1090 nm), read the current polarization state, stabilize to azimuth -147 deg and ellipticity 8 deg with stopping threshold of 0.5 deg, and re-read the polarization state for verification. The polarization stabilization is implemented using a multi-stage gradient descent procedure that iteratively adjusts the four piezo control codes while monitoring the polarization state until convergence criteria are met.

Fig. 11(b) shows the results given the input prompt, including a series of deliberate fiber perturbations to demonstrate system robustness. Starting from a random initial state far from the target ($\psi = 39.33^\circ$, $\chi = -1.05^\circ$), the system converges to target values ($\psi = -47^\circ$, $\chi = 8^\circ$), achieving the stopping criterion (angular error $< 5^\circ$) after 12 iteration, with an average iteration time of 0.23 sec. For each optimization iteration, the controller performs multiple polarimeter readings to decide the actuation direction: for each piezo channel, it applies one small step forward and one small step backward, measures the resulting polarization states, and executes an actuation step in the direction that most significantly reduces the angular error relative to the target. During convergence, the system successfully recovers from multiple perturbations, including manual fiber disturbances that temporarily shift the polarization by over 40° (visible at iterations 4 and 9). The piezo control voltages display smooth optimization trajectories with significant adjustments across all channels: starting from the initialization at 2.5 V, channels 1, 2, and 4 increase to 2.75 V, 2.77 V, and 2.81 V respectively, while channel 3 decreases slightly to 2.18 V during the optimization process.

E. DAS-enabled Fiber Sensing and Event Detection

In the final case study, we show that AgentOptics can also assist in monitoring fiber conditions using distributed acoustic sensing (DAS) and in determining whether a potential fiber cut event may occur that could affect optical link transmission performance. To support agentic workflow supporting DAS operation, we develop MCP tools for an NEC Spectral LS3300 DAS interrogator, which is set up to monitor a 27.4 km field fiber, as shown in Fig. 12(a). The MCP tools support DAS vibration monitoring over a specified time window and retrieval of the corresponding waterfall plot images. A waterfall plot shows vibration intensity along the sensing fiber over time, with distance along the fiber on the horizontal axis, time on the vertical axis, and color indicating vibration amplitude or strain rate. This representation enables rapid identification of the location, timing, and strength of vibration events. The returned images are autonomously analyzed by an LLM to determine potential fiber cut events based on abnormal vibration patterns.

Without domain-specific guidance, AgentOptics often fails to accurately identify fiber cut events due to limited knowledge of fiber sensing characteristics. To address this challenge, we apply prompt engineering [56] to supply additional domain knowledge related to fiber-sensing waterfall plots, thereby enhancing the reasoning capability of AgentOptics for DAS

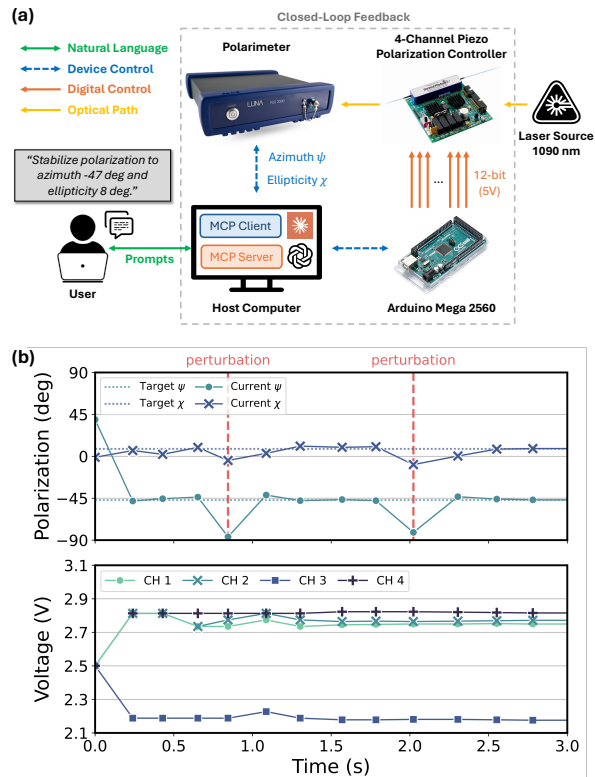


Fig. 11: (a) Experimental setup and control architecture for fiber link polarization stabilization using AgentOptics. (b) Closed-loop polarization stabilization results with deliberate fiber perturbations, showing polarization state and piezo controller actuation over time.

analysis. In addition to requesting a determination of whether a given waterfall plot indicates an impending fiber cut, we provide background information in the prompt describing characteristic pre-cut waterfall plot patterns. This information is combined with the fiber cut determination request and the corresponding waterfall plot and fed into the LLM.

We further validate this prompt engineering approach for fiber cut prediction using a previously recorded real-world fiber cut event that occurred on a 53 km field-deployed fiber. Figs. 12(c)–(e) compare the LLM-based waterfall analysis with and without prompt engineering under three scenarios: a stable environment, a slight fiber perturbation event induced by manually agitating the fiber to generate horizontal bright lines in the waterfall plot, and a real fiber cut event recorded on a 53 km field fiber loop. The prompt provides explicit descriptions of fiber cut signatures in waterfall plots, such as: “A fiber cut event is detected when fiber agitation produces multiple vertical streaks, or when unequal brightness between the top and bottom vertical lines indicates a power discontinuity.” As shown in Figs. 12(c)–(e), incorporating prompt engineering enables the LLM to reliably detect fiber cut events, thereby demonstrating AgentOptics is capable as a fully MCP-driven, LLM-in-the-loop fiber sensing and monitoring framework that can help prevent data traffic disruption caused by fiber cuts.

VII. CONCLUSIONS

In this paper, we presented AgentOptics, an MCP-based framework for autonomous and scalable control of optical

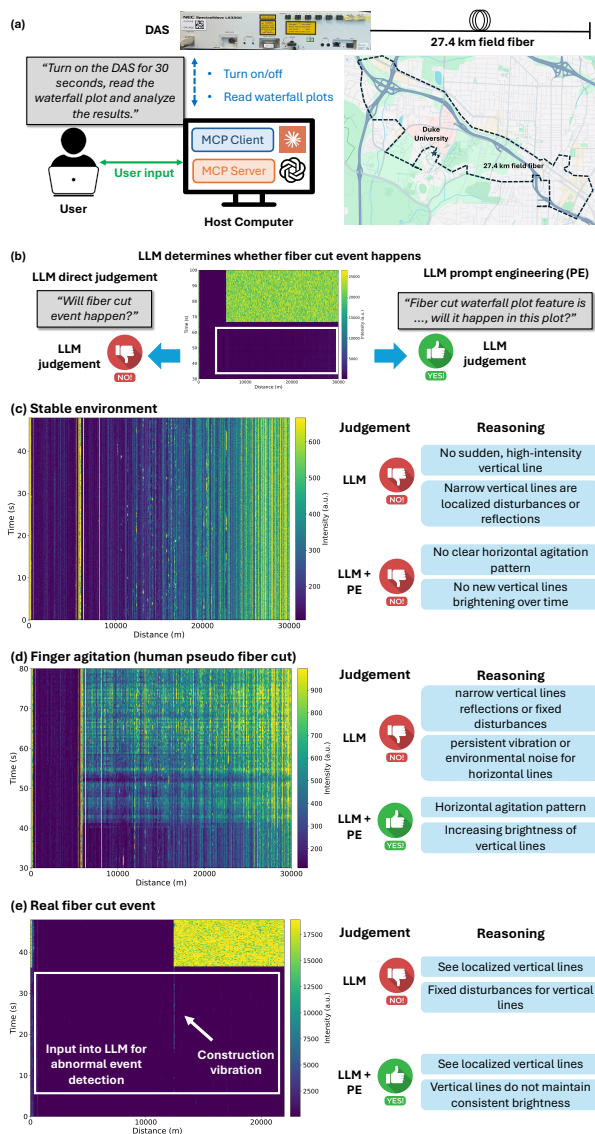


Fig. 12: (a) Experimental setup and workflow for AgentOptics-enabled fiber monitoring using distributed fiber sensing (DAS). (b) LLM-based reasoning and prompt engineering (PE) for automated event interpretation on the DAS waterfall plot analysis for (c) a stable environment, (d) human-induced pseudo fiber agitation, and (e) a real fiber cut event.

devices and systems. AgentOptics implements 64 standardized tools across eight physical devices and is systematically evaluated using a 410-task benchmark conducted on real hardware. We assess performance using five commercial online and three locally deployed open-source LLMs, and compare against the direct LLM-based code generation baselines. Overall, AgentOptics achieves task success rates of 99.0% and 87.7% with online and locally deployed LLMs, significantly outperforming the direct code-generation approaches and demonstrating strong robustness across model types. We further validate AgentOptics through five representative case studies from DWDM signal provisioning and monitoring to DAS-based fiber sensing with LLM-assisted event detection. These case studies collectively demonstrate AgentOptics’s ability to coordinate heterogeneous optical devices, execute closed-

loop optimization, and enable intelligent orchestration in real-world testbeds. Future work will expand the AgentOptics MCP toolset to incorporate broader classes of optical and hybrid wireless-optical systems, improve robustness for large-scale and long-horizon orchestration tasks, and incorporate enhanced safety mechanisms and cost-efficient deployments. We also plan to enhance AgentOptics in more complex operational environments to further advance autonomous optical network control and management.

APPENDIX

A. DWDM Link Setup and Performance Monitoring

Prompt: “Add a WSS connection named ‘ARoF’ with frequency from 193900 GHz to 194450 GHz with attenuation of 19.5 dB on the MUX side, using input port 1 and connection ID 1. Add a WSS connection named ‘CFP2’ with frequency from 193400 GHz to 193700 GHz with attenuation of 5 dB on the MUX side, using input port 20 and connection ID 2. Set the OSA start wavelength to 1540nm and stop wavelength to 1550nm. Add a WSS connection named ‘ARoF’ from 193900 GHz to 194450 GHz with attenuation of 5 dB on the DEMUX side, using output port 1 and connection ID 1. Add a WSS connection named ‘CFP2’ from 193400 GHz to 193700 GHz with attenuation of 5 dB on the DEMUX side, using output port 20 and connection ID 2. Set the CFP2 frequency to 193500000 MHz. Set the ARoF TX current to 99 mA and bias voltage to -0.9 V.”

B. Wideband 5G ARoF Link Characterization

Prompt: “You are an automated experiment controller tasked with finding the optimal bias voltage for an analog radio-over-fiber (ARoF) link. The testbed consists of an RFSoc that generates and receives RF signals routed through optical transceivers, with system parameters fixed as follows: RF bandwidth at 400 MHz, DAC NCO at 600 MHz, ADC NCO at -600 MHz, RF attenuation at 0 dB, and bias current at 99 mA. Using the AgentOptics MCP server, sweep the bias voltage from -1.5 V to 0 V in steps of 0.1 V, and at each bias point use the ‘rfsoc link tester’ MCP server to measure EVM, SNR, and BER for three modulation schemes: QPSK, 16QAM, and 64QAM. Once all measurements are collected, generate SNR-vs-bias and BER-vs-bias plots for all modulation schemes, and write the results into three markdown files, each organized as a table with bias voltage and per-modulation metric values clearly presented.”

C. Adaptive Channel Configuration and GSNR Optimization on Multi-Span Optical Links

Prompt: “Set a new CFP channel output power to -10 dBm, add an ROADM 2 WSS single connection for a 400 GbE channel at 195.5 THz, and record the CFP input power and pre-FEC BER. The current link is CFP transmitter → ROADM 1 booster → 20 km fiber → ROADM 2 booster → 27 km field fiber → ROADM 3 preamp → CFP receiver. Optimize the CFP launching power from -15 to 0 dBm to minimize the pre-FEC BER of the added CFP channel without adjusting any

ROADM gains, ensuring the received power of the new CFP channel remains below 0dBm. An existing CFP channel is already stable; its pre-FEC BER must not change significantly during optimization, and the ROADM 2 demux input power for channels 1–20 must not vary by more than ± 0.5 dB before and after optimization. Record each step, including pre-FEC BER for both the existing and newly added CFP channels, to determine the optimal launching power.”

D. Polarization Monitoring and Stabilization

Prompt: “Configure POD2000 at 1090 nm wavelength, get the current polarization state, then stabilize the polarization to azimuth -47 deg and ellipticity 8 deg with a stop threshold of 0.5 deg, and verify the result.”

E. DAS-Enabled Fiber Sensing and Event Detection

Prompt: “A fiber cut event can occur under two conditions: (1) fiber agitation, which appears as horizontal lines in the waterfall plot even when they are not dominant; this agitation is often accompanied by multiple vertical lines, indicating a potential fiber cut event; and (2) a mismatch in brightness between the vertical lines at the top and bottom of the plot, which may also suggest a fiber cut. Based on these criteria, does this waterfall plot indicate a fiber cut event?”

REFERENCES

- [1] H. Nishizawa, G. Borraccini, T. Sasai, Y.-K. Huang, T. Mano, K. Anazawa, M. Namiki, S. Usui, T. Matsumura, Y. Sone *et al.*, “Semi-automatic line-system provisioning with an integrated physical-parameter-aware methodology: Field verification and operational feasibility,” *IEEE/Optica J. Opt. Commun. Netw.*, vol. 16, no. 9, pp. 894–904, 2024.
- [2] H. Nishizawa, T. Mano, T. Ferreira de Lima, Y.-K. Huang, Z. Wang, W. Ishida, M. Kawashima, E. Ip, A. D’Amico, S. Okamoto *et al.*, “Fast WDM provisioning with minimal probing: The first field experiments for DC exchanges,” *IEEE/Optica J. Opt. Commun. Netw.*, vol. 16, no. 2, pp. 233–242, 2024.
- [3] T. Sasai, G. Borraccini, Y.-K. Huang, H. Nishizawa, Z. Wang, T. Chen, Y. Sone, M. Takahashi, T. Matsumura, M. Nakamura *et al.*, “Optical link tomography: First field trial and 4D extension,” *IEEE J. Lightwave Technol.*, vol. 43, no. 24, pp. 10776–10787, 2025.
- [4] Z. Wang, A. Raj, Y.-K. Huang, E. Ip, G. Borraccini, A. D’Amico, S. Han, Z. Qi, G. Zussman, K. Asahi *et al.*, “Toward intelligent and efficient optical networks: Performance modeling, co-existence, and field trials,” in *Proc. OECC/PSC’25*, 2025.
- [5] A. Ferrari, J. Kunderát, E. Le Rouzic, M. Filer, A. Campanella, A. D’Amico, K. Balasubramanian, Y. Yin, O. Havliš, M. Hažlinský *et al.*, “The GNPY open source library of applications for software abstraction of WDM data transport in open optical networks,” in *Proc. IEEE NetSoft’20*, 2020.
- [6] J. Yu, T. Chen, C. Gutterman, S. Zhu, G. Zussman, I. Seskar, and D. Kilper, “COSMOS: Optical architecture and prototyping,” in *Proc. IEEE/OSA OFC’19*, 2019.
- [7] C. Simon, “Towards a global quantum network,” *Nature Photonics*, vol. 11, no. 11, pp. 678–680, 2017.
- [8] A. Sevinçer, A. Bhattarai, M. Bilgi, M. Yuksel, and N. Pala, “LIGHT-NETS: Smart LIGHTing and mobile optical wireless NETWORKS: A survey,” *IEEE Commun. Surv. Tutor.*, vol. 15, no. 4, pp. 1620–1641, 2013.
- [9] G. Borraccini, S. Straullu, A. D’Amico, A. Nespola, S. Piciaccia, A. Tanzi, G. Galimberti, and V. Curri, “Autonomous raman amplifiers in multi-band software-defined optical transport networks,” *IEEE/Optica J. Opt. Commun. Netw.*, vol. 13, no. 10, pp. E53–E62, 2021.
- [10] D. Raychaudhuri, I. Seskar, G. Zussman, T. Korakis, D. Kilper, T. Chen, J. Kolodziejski, M. Sherman, Z. Kostic, X. Gu *et al.*, “Challenge: COSMOS: A city-scale programmable testbed for experimentation with advanced wireless,” in *Proc. ACM MobiCom’20*, 2020.
- [11] T. Chen, J. Yu, A. Minakhmetov, C. Gutterman, M. Sherman, S. Zhu, S. Santaniello, A. Biswas, I. Seskar, G. Zussman *et al.*, “A software-defined programmable testbed for beyond 5G optical-wireless experimentation at city-scale,” *IEEE Network*, vol. 36, no. 2, pp. 90–99, 2022.
- [12] R. Casellas, R. Martinez, R. Vilalta, and R. M. noz, “Overview of SDN control of multiband over SDM optical networks with physical layer impairments,” *J. Opt. Commun. Netw.*, vol. 17, no. 2, pp. A165–A177, 2025.
- [13] X. Hou, Y. Zhao, Y. Liu, Z. Yang, K. Wang, L. Li, X. Luo, D. Lo, J. Grundy, and H. Wang, “Large language models for software engineering: A systematic literature review,” *ACM Trans. Softw. Eng. Methodol.*, vol. 33, no. 8, 2024.
- [14] “Model context protocol,” <https://modelcontextprotocol.io>, 2025.
- [15] J. Yang, C. E. Jimenez, A. Wettig, K. Lieret, S. Yao, K. Narasimhan, and O. Press, “SWE-agent: agent-computer interfaces enable automated software engineering,” in *Proc. NeurIPS’24*, 2024.
- [16] O. Wijerathne, A. Nimasha, D. Fernando, N. de Silva, and S. Perera, “ScheduleMe: Multi-agent calendar assistant,” *arXiv:2509.25693*, 2025.
- [17] X. Wang, X. Ling, K. Li, G. Yin, L. Zhang, J. Wu, A. Wang, and W. Wang, “LLM and agent-driven data analysis: A systematic approach for enterprise applications and system-level deployment,” *arXiv:2511.17676*, 2025.
- [18] M. Xu, D. Niyato, J. Kang, Z. Xiong, S. Mao, Z. Han, D. I. Kim, and K. B. Letaief, “When large language model agents meet 6G networks: Perception, grounding, and alignment,” *IEEE Wireless Commun.*, vol. 31, no. 6, pp. 63–71, 2024.
- [19] N. Yang, G. Lyu, M. Ma, Y. Lu, Y. Li, Z. Gao, H. Ye, J. Zhang, T. Chen, and Y. Chen, “IoT-MCP: Bridging LLMs and IoT systems through model context protocol,” in *Proc. ACM WINTeCH’25*, 2025.
- [20] Y. Wang, W. Ye, Y. He, Y. Chen, G. Qu, and A. Li, “MCP4EDA: LLM-powered model context protocol RTL-to-GDSII automation with backend aware synthesis optimization,” *arXiv:2507.19570*, 2025.
- [21] A. Sharma, Y. Fu, V. Ansari, R. Iyer, F. Kuang, K. Mistry, R. I. Aishy, S. Ahmad, J. Matres, D. R. Englund *et al.*, “AI agents for photonic integrated circuit design automation,” *APL Machine Learning*, vol. 3, no. 4, 2025.
- [22] Y. Wang, C. Zhang, J. Li, Y. Pang, L. Zhang, M. Zhang, and D. Wang, “AlarmGPT: an intelligent alarm analyzer for optical networks using a generative pre-trained transformer,” *J. Opt. Commun. Netw.*, vol. 16, no. 6, pp. 681–694, 2024.
- [23] Y. Pang, M. Zhang, Y. Liu, X. Li, Y. Wang, Y. Huan, Z. Liu, J. Li, and D. Wang, “Large language model-based optical network log analysis using LLaMA2 with instruction tuning,” *J. Opt. Commun. Netw.*, vol. 16, no. 11, pp. 1116–1132, 2024.
- [24] Y. Zhang, Q. Qiu, X. Liu, D. Fu, X. Liu, L. Fei, Y. Cheng, L. Yi, W. Hu, and Q. Zhuge, “First field-trial demonstration of L4 autonomous optical network for distributed AI training communication: An LLM-powered multi-AI-agent solution,” *arXiv:2504.01234*, 2025.
- [25] X. Liu, Q. Qiu, Y. Zhang, Y. Cheng, L. Yi, W. Hu, and Q. Zhuge, “First field trial of LLM-powered AI agent for lifecycle management of autonomous driving optical networks,” in *Proc. IEEE/Optica OFC’25*, 2025.
- [26] “AgentOptics: Agentic ai for scalable and robust optical systems control,” <https://github.com/functions-lab/AgentOptics>, 2026.
- [27] T. Schick, J. Dwivedi-Yu, R. Dessí, R. Raileanu, M. Lomeli, E. Hambro, L. Zettlemoyer, N. Cancedda, and T. Scialom, “Toolformer: Language models can teach themselves to use tools,” in *Proc. NeurIPS’23*, 2023.
- [28] S. Yao, J. Zhao, D. Yu, N. Du, I. Shafraan, K. Narasimhan, and Y. Cao, “ReAct: Synergizing reasoning and acting in language models,” *arXiv:2210.03629*, 2022.
- [29] L. Gao, A. Madaan, S. Zhou, U. Alon, P. Liu, Y. Yang, J. Callan, and G. Neubig, “PAL: Program-aided language models,” in *Proc. ICML’23*, 2023.
- [30] Y. Shen, K. Song, X. Tan, D. Li, W. Lu, and Y. Zhuang, “HuggingGPT: solving AI tasks with ChatGPT and its friends in Hugging Face,” in *Proc. NeurIPS’23*, 2023.
- [31] B. Breen, M. D. Tredici, J. McCarran, J. A. Mijares, W. W. Yin, K. Sulimany, J. M. Taylor, F. H. L. Koppens, and D. Englund, “Ax-prover: A deep reasoning agentic framework for theorem proving in mathematics and quantum physics,” *arXiv:2510.12787*, 2025.
- [32] J. Qiu, J. Shi, X. Juan, Z. Zhao, J. Geng, S. Liu, H. Wang, S. Wu, and M. Wang, “Physics supernova: AI agent matches elite gold medalists at IPHO 2025,” *arXiv:2509.01659*, 2025.
- [33] J. Chen, W. Chen, J. Du, J. Hu, Z. Jiang, A. Jie, X. Jin, X. Jin, C. Li, W. Shi *et al.*, “Seed-prover 1.5: Mastering undergraduate-level theorem proving via learning from experience,” *arXiv:2512.17260*, 2025.

- [34] D. Brodimas, A. Birbas, D. Kaposos, and S. Denazis, "Intent-based infrastructure and service orchestration using agentic-AI," *IEEE Open J. Commun. Soc.*, vol. 6, pp. 7150–7168, 2025.
- [35] X. Wu, Y. Wang, J. Farooq, and J. Chen, "LLM-driven agentic AI approach to enhanced O-RAN resilience in next-generation networks," in *Proc. IEEE INFOCOM'25 Workshops*, 2025.
- [36] Y. Zhang, Y. Song, Y. Pang, S. Li, X. Jiang, Y. Wang, J. Li, M. Zhang, and D. Wang, "Design and evaluation of an LLM-based agent for QoT estimation and performance optimization in optical networks," *IEEE Open J. Commun. Soc.*, vol. 6, pp. 7470–7484, 2025.
- [37] Y. Zhang, Q. Qiu, X. Liu, X. Yu, D. Fu, X. Liu, Z. Wang, H. Lin, Y. Chen, L. Yi, W. Hu, and Q. Zhuge, "AI agent for autonomous optical networks: architectures, technologies, and prospects [invited tutorial]," *J. Opt. Commun. Netw.*, vol. 18, no. 2, pp. A159–A178, 2026.
- [38] N. Di Cicco, M. Ibrahim, S. Troia, F. Musumeci, and M. Tornatore, "Open implementation of a large language model pipeline for automated configuration of software-defined optical networks," in *Proc. ECOC'24*, 2024.
- [39] C. Sun, X. Yang, N. D. Cicco, R. Ayassi, V. V. Garbhapu, P. A. Stavrou, M. Tornatore, G. Charlet, and Y. Pointurier, "Experimental demonstration of local AI-agents for lifecycle management and control automation of optical networks," *IEEE/Optica J. Opt. Commun. Netw.*, vol. 17, no. 8, pp. C82–C92, 2025.
- [40] Z. Wang, D. C. Kilper, and T. Chen, "Open EDFA gain spectrum dataset and its applications in data-driven EDFA gain modeling," *IEEE/Optica J. Opt. Commun. Netw.*, vol. 15, no. 9, pp. 588–599, 2023.
- [41] Z. Wang, Y.-K. Huang, S. Han, T. Wang, D. Kilper, and T. Chen, "Multi-span optical power spectrum prediction using ML-based EDFA models and cascaded learning," in *Proc. IEEE/Optica OFC'24*, 2024.
- [42] Z. Wang, A. Raj, G. Borraccini, S. Han, Y.-K. Huang, T. Wang, M. Ruffini, D. Kilper, and T. Chen, "Scalable machine learning models for optical transmission system management," in *Proc. IEEE/Optica OFC'25*, 2025, pp. M1J–3.
- [43] Z. Wang, A. D'Amico, G. Borraccini, A. Raj, Y.-K. Huang, S. Han, T. Wang, M. Ruffini, D. Kilper, and T. Chen, "Scalable ml models and cascaded learning for efficient multi-span osnr and gsnr prediction," *IEEE/Optica J. Opt. Commun. Netw.*, vol. 18, no. 1, pp. A88–A99, 2025.
- [44] H. Nishizawa, T. Mano, T. Ferreira de Lima, Y.-K. Huang, Z. Wang, W. Ishida, M. Kawashima, E. Ip, A. D'Amico, S. Okamoto *et al.*, "Fast WDM provisioning with minimal probing: the first field experiments for DC exchanges," *IEEE/Optica J. Opt. Commun. Netw.*, vol. 16, no. 2, pp. 233–242, 2024.
- [45] S. Xie, R. Raj, D. Briantcev, Z. Wang, T. Chen, and D. Kilper, "WDM system stimulated raman scattering spectrum and tilt prediction using CNN-based transfer learning," in *Proc. IEEE ONDM'25*, 2025.
- [46] A. Raj, Z. Wang, F. Slynne, T. Chen, D. Kilper, and M. Ruffini, "Multi-span optical power spectrum evolution modeling using ML-based multi-decoder attention framework," in *Proc. ECOC'24*, 2024.
- [47] Z. Wang, Y.-K. Huang, S. Han, T. Wang, D. Kilper, and T. Chen, "Multi-span optical power spectrum prediction using ML-based EDFA models and cascaded learning," in *Proc. IEEE/Optica OFC'24*, 2024.
- [48] Z. Wang, E. Akinrintoyo, D. Kilper, and T. Chen, "Optical signal spectrum prediction using machine learning and in-line channel monitors in a multi-span ROADM system," in *Proc. ECOC'22*, 2022.
- [49] Z. Wang, Y.-K. Huang, E. Ip, Z. Qi, G. Zussman, D. Kilper, K. Asahi, H. Kageshima, Y. Aono, and T. Chen, "Field trial of coexistence and simultaneous switching of real-time fiber sensing and coherent 400 GbE in a dense urban environment," *IEEE/Optica J. Lightwave Technol.*, vol. 42, no. 4, pp. 1304–1311, 2023.
- [50] B. Rozière, J. Gehring, F. Gloeckle, S. Sootla, I. Gat, X. E. Tan, Y. Adi, J. Liu, R. Sauvestre, T. Remez, J. Rapin, A. Kozhevnikov, I. Evtimov, J. Bitton, M. Bhatt, C. C. Ferrer, A. Grattafiori, W. Xiong, A. Défossez, J. Copet, F. Azhar, H. Touvron, L. Martin, N. Usunier, T. Scialom, and G. Synnaeve, "Code Llama: Open foundation models for code," *arXiv:2308.12950*, 2024.
- [51] E. J. Hu, Y. Shen, P. Wallis, Z. Allen-Zhu, Y. Li, S. Wang, L. Wang, W. Chen *et al.*, "LoRA: Low-rank adaptation of large language models," *ICLR*, vol. 1, no. 2, p. 3, 2022.
- [52] W. Cheng, Z. Gao, J. Guajardo, H. Beshary, A. M. Niknejad, and T. Chen, "SPEAR+: Streaming-based multi-channel SDR implementation using the RFSoc platform," in *Proc. IEEE MILCOM'25*, 2025.
- [53] H. Ji, Z. Wang, X. Li, J. Li, R. R. Unnithan, Y. Su, W. Hu, and W. Shieh, "Photonic integrated self-coherent homodyne receiver without optical polarization control for polarization-multiplexing short-reach optical interconnects," *IEEE/Optica J. Lightw. Technol.*, vol. 41, no. 3, pp. 911–918, 2023.
- [54] X. Fu, Z. Deng, Q. Wei, and Z. Li, "Polarization fading suppression in distributed interferometric sensing by matched interference between polarization-switched pulses," *Opt. Express*, vol. 30, no. 11, pp. 19705–19715, 2022.
- [55] S.-H. Yin, T.-W. Luo, W.-J. Jiang, X.-Y. Liu, Y.-F. Yu, Z.-J. Wei, T.-M. Zhao, J.-B. Fang, and J.-D. Wang, "Polarization compensation for entanglement-based quantum key distribution," *Opt. Express*, vol. 33, no. 18, pp. 38431–38439, 2025.
- [56] T. Shin, Y. Razeghi, R. L. Logan IV, E. Wallace, and S. Singh, "Auto-prompt: Eliciting knowledge from language models with automatically generated prompts," *arXiv:2010.15980*, 2020.